Tensile Deformation Temperature Impact on Microstructure and Mechanical Properties of AISI 316LN Austenitic Stainless Steel

Yi Xiong, Tiantian He, Yan Lu, Fengzhang Ren, Alex A. Volinsky, and Wei Cao

Uniaxial tensile tests were conducted on AISI 316LN austenitic stainless steel from − 40 to 300 °C at a rate of 0.5 mm/min. Microstructure and mechanical properties of the deformed steel were investigated by optical, scanning and transmission electron microscopies, x-ray diffraction, and microhardness testing. The yield strength, ultimate tensile strength, elongation, and microhardness increase with the decrease in the test temperature. The tensile fracture morphology has the dimple rupture feature after low-temperature deformations and turns to a mixture of transgranular fracture and dimple fracture after high-temperature ones. The dominating deformation microstructure evolves from dislocation tangle/slip bands to large deformation twins/slip bands with temperature decrease. The deformation-induced martensite transformation can only be realized at low temperature, and its quantity increases with the decrease in the temperature.

1. Introduction

Endowed with intergranular corrosion resistance, high tensile strength at elevated temperature, and creep strength, the 316LN austenitic stainless steel is widely used in nuclear power plants as a structural material at crucial places such as the main pipeline, heat exchanger, and bolted flange connections (Ref 1, 2). It is well known that solid-state transformations do not take place during heating processes. For this reason, forging is needed to improve microstructure and mechanical properties of 316LN austenitic stainless steel. However, the narrow window of the forging temperature and relatively high deformation resistance limit its wide applications in the 316LN austenitic stainless steel treatments. For these reasons, many researches were mainly focused on rheological behavior and microstructure evolution of 316LN austenitic stainless steel during hot deformations. Poliak et al. (Ref 3-5) studied dynamic recrystallization behavior of 316LN austenitic stain-less steel during hot deformation. There was a deflection in the true stress–strain curves, and the deflection point represented the beginning of dynamic recrystallization. Byun et al. (Ref 6) studied the impacts of irradiation, test temperature and strain on the deformation microstructure of 316LN austenitic stainless steel. Deformation microstructure changed from a dominant feature of dislocation tangle to the large stacking fault/twin band when increasing radiation dose and strain or decreasing test temperature. The tensile deformation behavior of 316LN austenitic stainless steel was also revealed at room and high temperatures (Ref 7). These findings provided useful guidelines for processing and service of 316LN austenitic stainless steel components at high temperature.

Early studies showed the yield strength was slightly influenced by strain rate and temperature, but ultimate tensile strength was affected significantly during cryogenic tensile tests (Ref 8). Similar results were also observed in experiments with austenitic stainless steel plates (Ref 9). Behjati (Ref 10) stated that the yield strength is less vulnerable to the temperature, while the ultimate tensile strength is greatly influenced by temperature. In Ref 11-13, it has been generally found that the elongation of 316LN austenitic stainless steel at low temperature is much higher than that at room temperature. In spite of the prior works, however, there is a lack of systematic studies of the microstructure evolution of 316LN austenitic stainless steel in static or quasi-static conditions at operating temperature and low temperature. The deficient knowledge limits the application range of 316LN austenitic stainless steel. Additionally, the deformation-induced martensite transformation has not been considered during service time.

In this paper, uniaxial tensile tests from − 40 to 300 °C were conducted on 316LN austenitic stainless steel, and the corresponding microstructure evolution and mechanical properties changes were systematically investigated. The results discussed in this paper can provide useful experimental support for the development and applications of 316LN austenitic stainless steel.

Yi Xiong and **Fengzhang Ren**, School of Materials Science and Engineering, Henan University of Science and Technology, Luoyang 471023, China; and Collaborative Innovation Center of Nonferrous Metals, Luoyang 471023, China; **Tiantian He** and **Yan Lu**, School of Materials Science and Engineering, Henan University of Science and Technology, Luoyang 471023, China; **Alex A. Volinsky**, Department of Mechanical Engineering, University of South Florida, Tampa, FL 33620; and **Wei Cao**, Nano and Molecular Systems Research Unit, University of Oulu, 90014 Oulu, Finland. Contact e-mail: xy_hbdy@163.com.

2. Materials and Experimental Procedure

Vacuum induction furnace was used to manufacture the investigated 150 kg steel ingot with the following chemical composition (in wt.%): 0.01C, 0.49Si, 0.87Mn, 17.09Cr, 14.04 Ni, 2.56Mo, 0.14N, and Fe balance. The ingot was hot forged down to a 15-mm-thick slab. The slab was then heat-treated at 1050 °C for 2 h. After solution treatment, the tensile test specimens with a gage length of 15, 3 mm wide and 1 mm thick were prepared along the longitudinal direction, as shown in Fig. 1. The uniaxial tensile tests were conducted by using UTM4104 electronic universal testing machine with a sealed environmental chamber. The low temperature was adjusted with liquid nitrogen under flow control, while the high temperature was kept using a resistance heating wire. The test temperatures were − 40, − 20, 25 °C (room temperature), 100, 200 and 300 °C, respectively. The tensile rate was 0.5 mm/min. The morphology of the fracture surfaces was observed using a scanning electron microscope (SEM, JSM-5610LV), operated at 20 kV. The average dimple size was determined by intercept method. Microstructure characterization near tensile fracture zone was carried out via optical microscopy (OLYMPUS PMG3) and transmission electron microscopy (TEM, JEM-2010). For metallographic examination, samples were prepared by chemical corrosion using aqua regia. For the TEM study, mechanically thinned 50 μm disks were prepared using twin gun precision ion polishing system (Gatan, model 691). The operating voltage of TEM was 200 kV. The x-ray diffraction (XRD) experiments were carried out on the D/MAX 2400 x-ray diffractometer. The tube voltage and current were 35 kV and 40 mA, respectively. The $CuK_{\alpha 1}$ ($\lambda = 0.15406$ nm) beam was tuned with a diameter of ∼ 2 mm as the incident source. The scan angle range was 40-100° at a speed of 0.02°/s. Using the $(200)_\gamma$, $(220)_\gamma$, $(311)_\gamma$, $(200)_{\alpha'}$, $(211)_{\alpha'}$, $(220)_{\alpha'}$ reflections, the volume fraction of α'-martensite was calculated through the following equation:

$$V_\alpha = \frac{1/n \sum_{j=1}^n I_{\alpha'}^j / R_{\alpha'}^j}{1/n \sum_{j=1}^n I_{\alpha'}^j / R_{\alpha'}^j + 1/n \sum_{j=1}^n I_\gamma^j / R_\gamma^j} \quad \text{(Eq 1)}$$

Here, n, I, and R represent the diffraction number, diffraction intensity, and scattering factor, respectively. An average volume fraction of α'-martensite was determined based on three measurements. Microhardness was measured using the MH-3 Vickers microhardness tester with 200 g normal load and 10 s holding time. The microhardness was averaged from values given by fiv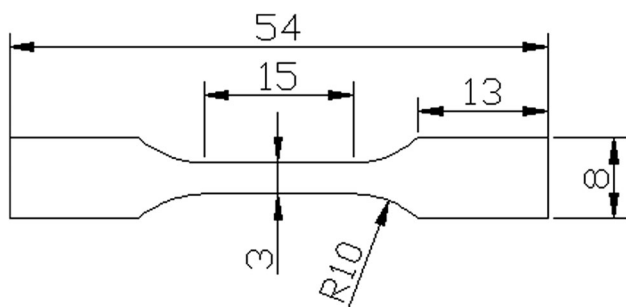e indentation measurements. After grinding and polishing the tensile fracture surface, the microhardness tests were carried out at 1 mm distance from the fracture surface.

3. Results

3.1 Temperature Dependence of Engineering Stress–Strain Curves

Figure 2 shows the engineering stress–strain curves of 316LN austenitic stainless steels under different temperatures. It can be seen that the curves are quite similar. The steel showed strong temperature dependences for the strength and elongation. As the test temperature decreased from 300 to − 40 °C, the ultimate tensile strength (UTS) and the yield strength (YS) increased by 84 and 67%, from 345 and 134 MPa to 635 and 224 MPa, respectively. As expected, the yield strength and ultimate tensile strength increased with the decrease in the test temperature. However, the speed of changes was different between the yield strength and ultimate tensile strength. Following the temperature decrease, the yield strength increased slightly, while the ultimate tensile strength increased rapidly. This is consistent with other studies (Ref 8-10). The elongation at − 40 °C was obviously higher than at 300 °C and enhanced from 37 to 92%. This is in line with similar observation as reported in Ref 11-13.

As shown in Fig. 3, both YS and UTS reversely increased with temperature. The strength properties (UTS) as well as the elongation were noticeably enhanced at lower test temperature. These increases can normally be due to the formation of face centered cubic (FCC) materials, at the present stage, the deformation-induced martensite (Ref 14-17). The volume fraction of martensite increases when lowering the test temperature (Ref 18), resulting in increases in the YS and the UTS due to composite strengthening by continuous refinement of the martensite and austenite mixture (Ref 19-21). The present results support the aforementioned claims. A large increase in elongation up to 92% indicates a deviation from the normal FCC material behavior. The UTS, YS, and elongation are found to increase with the martensite volume fraction. In
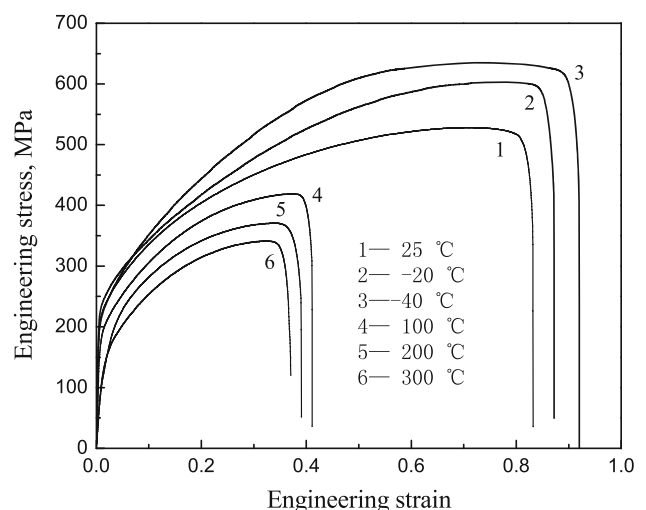

Fig. 1 Diagram of tensile test specimens

Fig. 2 Engineering stress–strain curves of 316LN austenitic stainless steels under different temperatures

general, the uniform elongation should increase when more stress-induced obstacles, such as large stacking faults, twins, and martensite laths are formed (Ref 19). During the deformation, less uniform elongation will be yielded when tangled dislocation networks are dominant.

3.2 Deformation Microstructure Near Tensile Fracture

Figures 4 and 5 show OM and TEM images of microstructure near the tensile fracture. After solution treatment, the microstructure was equiaxed austenite grains with the size of about 50 μm. Additionally, in local area a small amount of annealing twins was also observed as shown in Fig. 4(a). After room temperature tensile test, deformed grains with slide lines turned out (Fig. 4b). The direction of the slip bands was different among the grains, presenting a typical feature of
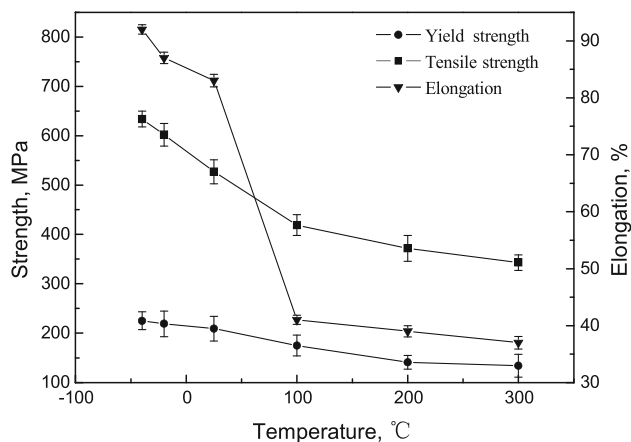

Fig. 3 Mechanical properties of the 316LN austenitic stainless steels under different temperatures

metals with low stacking fault energy (Ref 22, 23). When the temperature increased to 300 °C, the number of the slip bands reduced and a small amount of annealing twins turns up in the deformed grains. The degree of deformation was smaller than that at room temperature and the austenite grain size increased to 60-70 μm, as shown in Fig. 4(c). When the test temperature was tuned to − 40 °C, the number of slip bands obviously increased. Interactions happened between slip bands with different directions, resulting in elongated austenite grains. The martensitic structure was formed in the deformed microstructure. The deformation degree was higher than that at room temperature. The corresponding microstructure is identified in Fig. 4(d).

Figure 5(a) and (b) shows that at room temperature there was deformation mainly accomplished by slip bands and dislocation substructures, along with a small amount of deformation twins. Moreover, dislocations moved easily and were annihilated because of dislocation–dislocation interactions during the movement. This resulted in indistinct sliding boundaries and lowered dislocation density in steel, along with local area high-density dislocation loops and tangled networks. For example, this microstructure is observed at 300 °C in Fig. 5(c) and (d). Similar results for microstructure evolution of 316LN stainless steel during creep and fatigue were obtained by Prasad Reddy et al. (Ref 24). With the temperature reduced to − 40 °C, the deformed microstructure was similar with that at room temperature. Under this condition, while the quantities of slip bands and dislocation substructures declined slightly, the number of deformation twins increased rapidly. Meanwhile, deformation twins with different directions interacted, as seen in Fig. 5(e) and (f). The nucleation sites were provided by the joint impacts from the suppression of temperature rise of the samples at low test temperature and the twin dislocation intersection. As a result, the amount of martensite transformation increases.
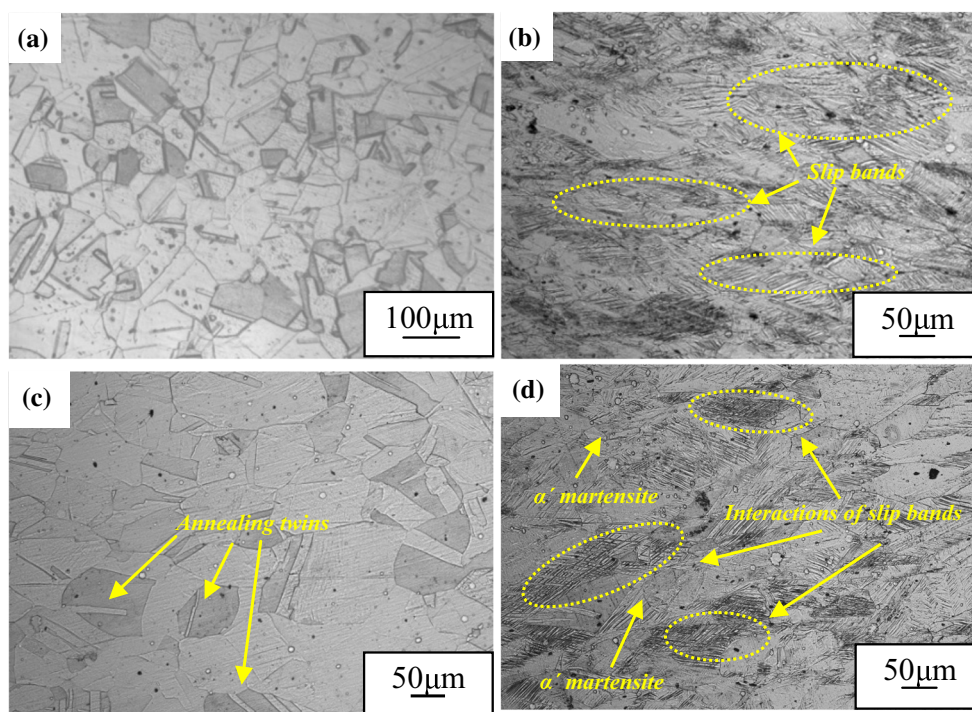

Fig. 4 OM images of microstructure near the tensile fracture: (a) before tensile; (b) room temperature (25 °C); (c) 300 °C; (d) − 40 °C
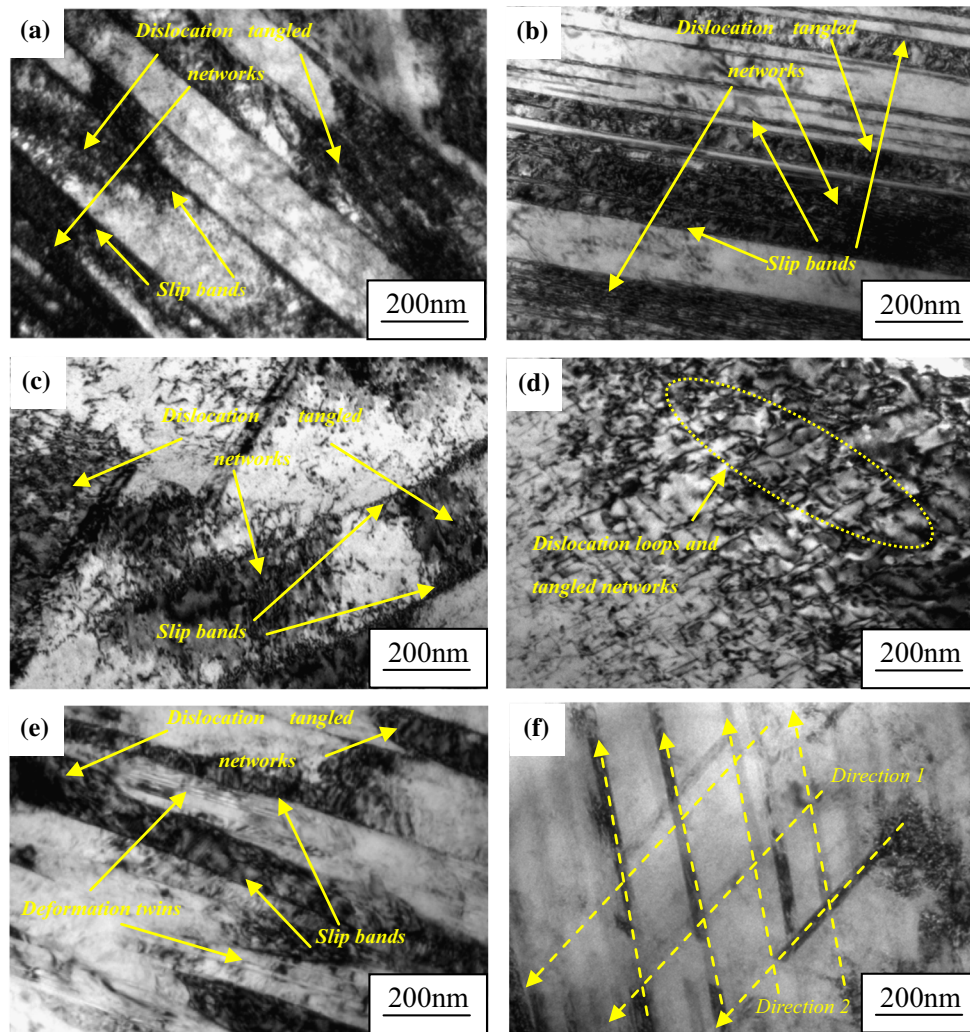
Fig. 5 TEM images of microstructure near the tensile fracture: (a) and (b) room temperature (25 °C); (c) and (d) 300 °C; (e) and (f) − 40 °C
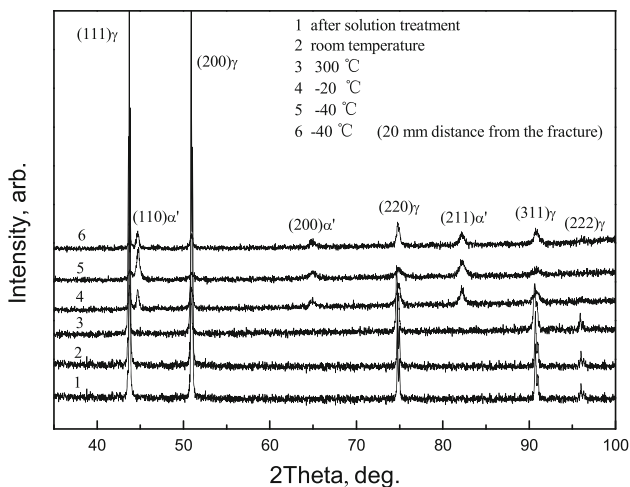

Fig. 6 XRD patterns of 316LN austenitic stainless steels after uni-axial tensile tests at different temperatures

3.3 XRD Analysis

The XRD patterns of 316LN austenitic stainless steel after uniaxial tensile tests at different temperatures are shown in

Fig. 6. Compared with the samples without deformation, no additional diffraction peaks were not found when the deformation temperature was above the room temperature. The deformation-induced martensitic transformation did not occur in the 316LN austenitic stainless steel after tensile deformation under this condition. As the temperature was reduced to − 20 and − 40 °C, diffraction peaks of the α'-martensite were present near the fracture surface of austenitic stainless steel. The fraction of α'-martensite transformation increased from 17.3% (− 20 °C) to 34.9% (− 40 °C). Meanwhile, deformed at − 40 °C, the amount of α'-martensite transformation was only 13.6% at the place $\sim$ 20 mm apart from the fracture surface. In fact, the deformation-induced martensitic transformation of 316LN austenitic stainless steel depends on strain, stress, strain rate, deformation temperature, and so on. Larger strain leads to more defects and easier martensite nucleation around the defects (Ref 25). Shrinivas et al. (Ref 26) stated that the martensite of 316L austenitic stainless steel nucleated mainly in the intersection area of the shear bands, as influenced by the stacking fault energy. Thus, in order to induce martensitic transformation, large strain should be applied to materials. In austenitic stainless steels the formation of martensite has been frequently observed during deformation at room temperature or below (Ref 27-29). In situ observations on Fe-Ni-Cr stainless
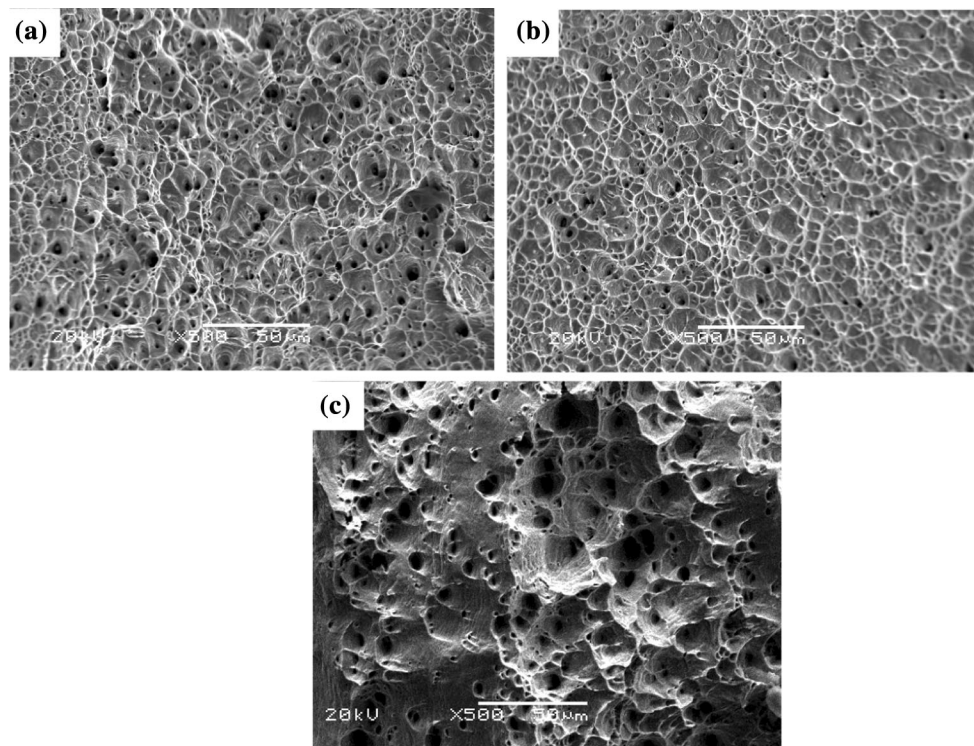
Fig. 7 Fractography of the 316LN austenitic stainless steels specimens tested at (a) − 20 °C; (b) room temperature (25 °C); (c) 300 °C (perpendicular to tensile direction)

steels showed that ε-martensite was formed along with stacking faults, while α′-martensite nucleation seemed to be associated with dislocation pile-ups (Ref 28, 29). In the present study, the deformation microstructure formed below room temperature is similar to the one reported in Ref 30. The amount of α′-martensite reversely increased with the temperature.

3.4 Fractography Analysis

Figure 7 shows the fractography of the 316LN austenitic stainless steel specimens tested at − 40, 25 °C (room temperature), and 300 °C. The SEM observations reveal that the fracture surfaces were completely ductile fracture at low temperature, but turned to a mixture of transgranular fracture and dimple fracture at high temperature. Very similar elongations over 80% were reached for the 316LN austenitic stainless steel treated equal to and below room temperature. The rates are much higher than these obtained for 100-300 °C, as shown in Fig. 2 and 3. The sharp decrease in the elongation at higher temperature is mainly due to the slow growth of the austenite grains. This weakens the binding force of the grain boundary and reduces the plasticity and toughness. Similar phenomenon was observed in Ref 7, where the elongation of 316LN austenitic stainless steel was about 40% at 100-700 °C. After treated at 300 °C, the fracture surface possesses several large and deep dimples with an average size of 12 ± 3 μm, and many small and shallow dimples (2 ± 1 μm). Choudhary et al. (Ref 31) stated that due to the dynamic strain aging, a low elongation of 316LN austenitic stainless steel was formed after deformation at 300 °C. When test temperature was reduced to 25 °C, a large amount of small and shallow dimples was observed on the fracture surface. In local area a small amount of large and deep dimples stayed at the bottom of the large dimples, denoting the

possible formation of secondary phase particles. Further decreasing the test temperature to −40 °C, the steel possesses large and deep dimples at the fracture surface and some secondary phase particles at the bottom of the dimples. This indicated that the 316LN austenitic stainless steel had better toughness via low-temperature deformation. The present results are consistent with the findings of Qin et al. (Ref 13). In their studies, the elongation tested at 77 K was higher than that at 300 K. Similar results were also reported in Ref 6 and attributed to substantial difference of strain hardening rate under different tensile temperatures. For the room temperature test, the elongation decreased by cold working. However, the trend does not apply to the cryogenic test, indicating the limited influences on cryogenic elongation at failure from the cold working. Ref 18 proposed a possible micromechanism to explain the void growth kinetics in austenitic stainless steels. Deformation-induced martensite affects the void growth characteristics by the factors of (i) retardation of void nucleation at early transformation softening and (ii) counteraction of the strain softening effect due to void growth by transformation hardening. The decrease in void growth can be explained by the obstruction of void growth due to rapid nucleation of deformation-induced martensite. The enhanced ductility is mainly due to the delayed necking because of the enhanced void nucleation and suppressed void growth (the presence of finer voids at −40 °C in Fig. 7). This phenomenon actually enables material to accommodate a large necking strain.

Figure 8 shows the surface morphology of the 316LN austenitic stainless steels specimens after tensile testing at room temperature. It can be seen that severe deformation occurred near to the fracture. The slip bands with different directions interacted with each other and formed wrinkles. Meanwhile, in local areas long and narrow cracks were observed, as indicated
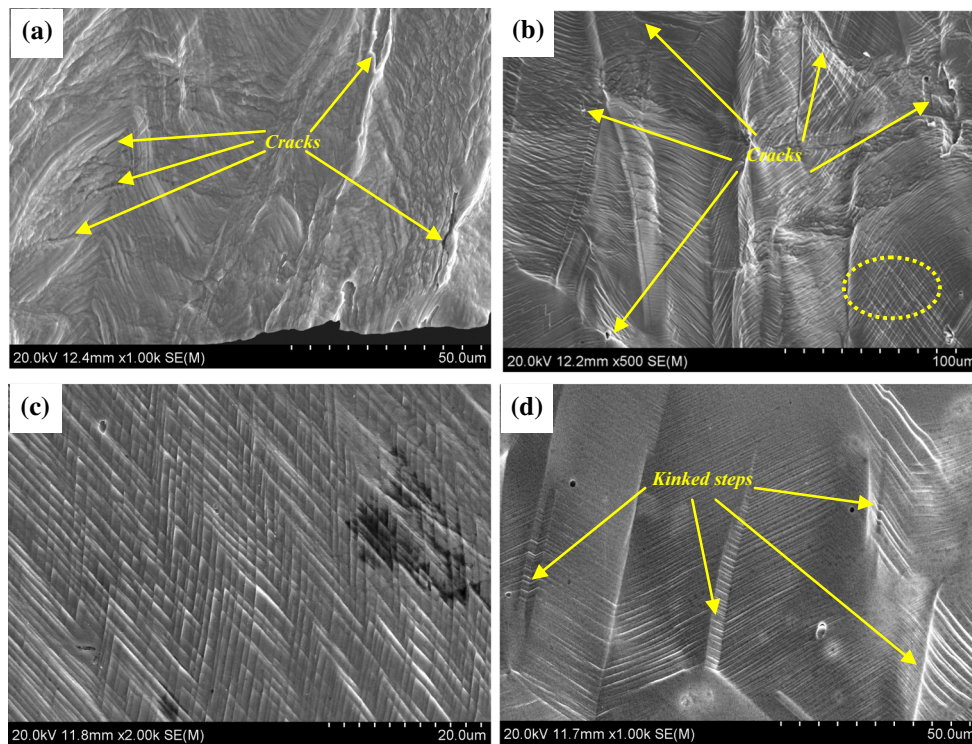
Fig. 8 Surface morphology of the 316LN austenitic stainless steels specimens after tensile at room temperature. (a) near the fracture; (b) 10 mm distance from the fracture; (c) the magnification of the elliptical area of (b); (d) 20 mm distance from the fracture (parallel to the tensile direction)

by the arrows in Fig. 8(a). Figure 8(b) depicts the surface morphology at a distance of 10 mm from the fracture zone. The wrinkles were formed, but the morphology was mainly wave texture. In the local area, a small amount of cracks existed and most slip bands in the austenite grains were parallel to each other. Figure 8(c) shows the magnification of the elliptical area in Fig. 8(b) with wrinkles. The deformation morphology of the 316LN austenitic stainless steel is 20 mm away from the fracture surface as shown in Fig. 8(d). The deformation in Fig. 8(d) was smaller than those in Fig. 8(a) and (d). The deformation morphology has the shape of parallel slip bands, and causes kink steps following its non-uniformity (arrows in Fig. 8d). From Fig. 8, it can be concluded that there exists big deformations close to the fracture surface. Meanwhile, more wrinkles can be formed and in local areas of cracks. The similar results were also found in Ref 32. It stated that the fracture failure of the 316LN austenitic stainless steel was attributed to the decrease of surface roughness and increase in extensive twinning. Similar phenomenon was observed in situ SEM tension test of high-nitrogen austenitic stainless steels (Ref 33). The formation of microcracks was due to additional slip systems as a result of the larger space between the slip bands. The surface morphology of the specimens after tensile testing at lower or higher temperature was similar to the room temperature results.

3.5 Microhardness

Figure 9 shows the microhardness of the 316LN austenitic stainless steels samples near tensile fracture. The microhardness increased with the decrease of the test temperature. Treated with temperature below 25 °C, the steel microhardness changed slowly. The microhardness decreased only by 9.1% from 396
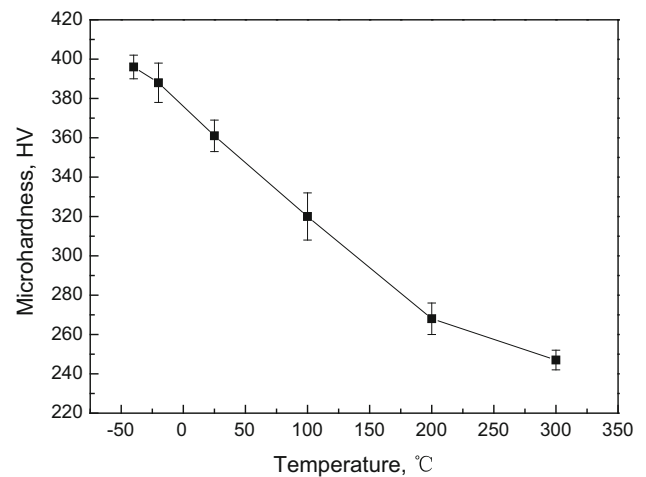

Fig. 9 Microhardness of the 316LN austenitic stainless steels samples near tensile fracture

HV (− 40 °C) to 360 HV (25 °C). Meanwhile, once the test temperature was higher than the room temperature, the change of the microhardness was sharp, and the value was reduced by 31.3%, from 360 HV (25 °C) to 247 HV (300 °C). The microhardness near the fracture surface at different test temperatures was obviously higher than that after solid solution treatment (170 HV). Compared with the original sample before deformation, the microhardness near the fracture zone increased by 133 and 45% when the test temperatures were − 40 °C and 300 °C. When the test temperature was below room temperature, the deformation microstructure was in the form of dislocation tangles and deformation twins. There were more

dislocation tangles closer to the fracture surface. Meanwhile, the interaction of the deformation twins in different orientations occurred, leading to the grain refinement of the austenite matrix structure (Fig. 4d). Besides, the deformation-induced martensite transformation occurred at low temperature and the amount of martensite transformation increased when the temperature dropped. This lead to the large increase of the microhardness near the fracture surface. Similar phenomenon was revealed for the microhardness of the 316LN austenitic stainless steel after tensile testing under temperature range of 25 to 1000 °C (Ref 7). In that study, the microhardness decreased with the tensile test temperature. However, when the temperature was higher than the room temperature, the deformation microstructure was primarily dislocation tangles and dynamic recovery occurred. Thus, with the combination effect of dislocation strengthening and dynamic recovery, the microhardness at 300 °C was only 247 HV, much lower than the value at – 40 °C (396 HV).

4. Discussion

The present study illustrates microstructure evolutions of 316LN austenitic stainless steel deformed at different uniaxial tensile test temperatures ranging from – 40 to 300 °C. Experimental results clearly demonstrate that the test temperature significantly affects deformed microstructure characteristics. Depending on the deformation temperature, two types of microstructure were formed after tensile testing at different temperatures. Dominant microstructure changed from dislocation tangle/slip bands to large deformation twins/slip bands with the decrease in the test temperature. At the elevated temperature (300 °C), deformation microstructure is consisted of tangled dislocations, indicating that cross-slip occurred during dislocation glide. After the test temperature dropped to room temperature (25 °C), the deformation was mainly accomplished by slip bands and dislocation substructures, along with a small amount of deformation twins. When the test temperature further decreased to – 40 °C, the number of deformation twins obviously increased and the distance of the deformation twins reduced.

Due to the martensitic transformation, the stress concentration during lower temperature tensile testing reduced and cracking was delayed. The deformation-induced martensite transformation occurred at the largest deformation area, which resulted in the strength increase. The deformation became more difficult. The deformation propagated to other areas without martensitic transformations and postponed the necking formation. The formation and transformation of martensite depended on the accumulation of the strain energy. Due to the transformation induced plasticity (TRIP) effect, the strength and elongation were improved. Sato (Ref 34) and Seetharaman (Ref 35) found two transformation mechanisms from austenite to martensite. (1) When the stacking fault energy of the base metal was below 18 mJ/m^2, the transformation of martensite follows: γ-austenite → ε-martensite → α′-martensite. (2) When the stacking fault energy of the base metal was higher than 18 mJ/m^2, the transformation of martensite turns to: γ-austenite → twin → α′-martensite. Previous researches (Ref 36, 37) showed that the stacking fault energy of 316LN austenitic stainless steels was about 10 mJ/m^2; thus, the transformation of martensite in 316LN austenitic stainless steel followed the first mechanism. However, the diffraction peak of

ε-martensite was not found in the present XRD patterns (Fig. 6), neither from TEM observations (Fig. 10). This indicated that α′-martensite was mainly formed in 316LN austenitic stainless steel after low-temperature tensile deformation. The content of ε-martensite was low, or ε-martensite transition phase eventually transformed to α′-martensite with more deformation. Moreover, austenite has coherent relation with martensite and high interfacial energy prevented crack propagation, resulting in elongation increase. With further strain increase and temperature decrease, the dislocation tangles aggravated which prevent the dislocation movement. In order to coordinate the severe plastic deformation, deformation twins were formed. Meanwhile, the subgrain orientation was altered, leading to release of stress concentration. Deformation twins were restricted and interacted with each other, which hindered dislocation motion, forming the twinning induced plasticity (TWIP) effect. The elongation was improved. Under the combination TRIP and TWIP effects, strength and elongation of 316LN austenitic stainless steel at low temperature are significantly higher than that at high temperature. As shown in Fig. 2, once the deformation twins were formed in 316LN austenitic stainless steel, the elongation was high. When the test temperature was below room temperature, the elongation was over 80%. Meanwhile, the elongation was reduced to 40% when the test temperature was higher than the room temperature. This was mainly due to microstructure changes. When the test temperature was below room temperature, deformation twins were formed and the amount of the deformation twins increased sharply with the test temperature decrease. Besides, the elongation improved by quantity of the martensite is also ascribed to the TRIP effect (Ref 38, 39). Under the comprehensive function of TRIP and TWIP effect, the elongation was remarkably increased when decreasing the test temperature. Meanwhile, the elongation of 316LN austenitic stainless steel significantly increases with the test temperature reduction. When the test temperature was above the room temperature, the microstructure was in the form of dislocation tangles and the deformation twin did not occur, leading to poor work-hardening capacity. As a result, the elongation was significantly reduced with the test temperature increase, as shown in Fig. 2.

Twinning can contribute to failure in two ways. For one thing, twinning increases strain hardening and hence accounts for higher ductility (Ref 40). Twins may act as a barrier and the dislocations pile up at the boundary, which increases the chance
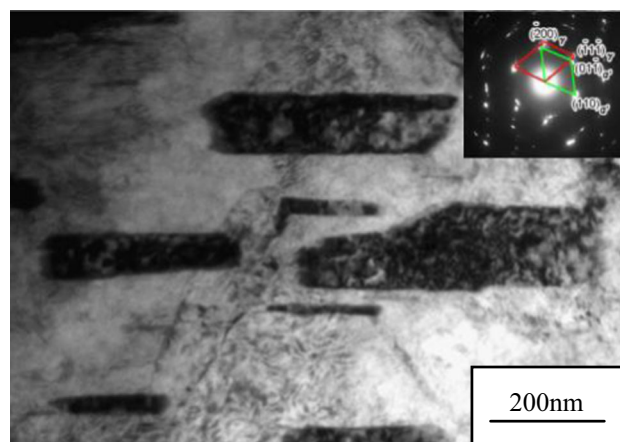

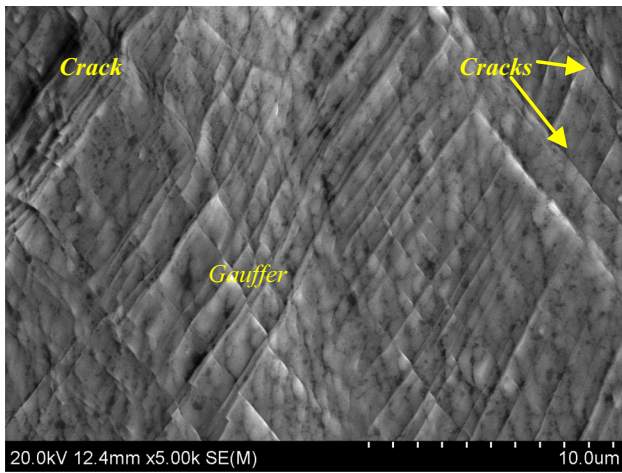**Fig. 10** Microstructure of the deformation-induced martensite

Fig. 11 Cracks and gauffers produced by the interaction between twins

of crack initiation at the sharp ends of the twin. Another possibility arises due to surface roughness (Ref 31), which results in further twinning in the adjacent grain, as seen in Fig. 11. Alternatively, it could lead to crack propagation along the grain boundary. Thus, the elongation of 316LN austenitic stainless steel at low temperature is significantly higher than that at high temperature mainly due to the formation of the deformation twin at low temperature, as shown in Fig. 2.

5. Conclusions

To conclude, the 316LN austenitic stainless steel after uniaxial tensile tests were conducted at the – 40 to 300 °C temperature range using electronic universal testing machine. The microstructure and mechanical properties were systematically characterized and analyzed. The results are as follows:

1. The deformation-induced martensite transformation only occurs at low temperature and increases in quantity following the temperature decrease. The corresponding yield strength, tensile strength, microhardness and elongation of 316LN austenitic stainless steel increase when tuning down the test temperature. The increase in the mechanical properties of 316LN austenitic stainless steel is attributed to the comprehensive function of TRIP and TWIP effect.
2. Deformation microstructure changed from a dislocation tangle/slip bands dominant to a large deformation twins/slip bands dominant with decreasing test temperature. The tensile fracture morphology is dimple rupture at low temperature and a mixture of transgranular fracture and dimple fracture at high temperature. However, the elongation at or below the room temperature can reach about two times higher than the one at high temperatures.

References

1. G.V. Prasad Reddy, R. Kannan, K. Mariappan, R. Sandhya, S. Sankaran, and K. BhanuSankaraRao, Effect of Strain Rate on Low Cycle Fatigue of 316LN Stainless Steel with Varying Nitrogen Content: Part-I, Cyclic Deformation Behavior, *Int. J. Fatigue*, 2015, **81**, p 299–308
2. G.V. Prasad Reddy, K. Mariappan, R. Kannan, R. Sandhya, S. Sankaran, and K. BhanuSankaraRao, Effect of Strain Rate on Low Cycle Fatigue of 316LN Stainless Steel with Varying Nitrogen Content: Part-II, Fatigue Life and Fracture, *Int. J. Fatigue*, 2015, **81**, p 309–317
3. E.I. Poliak and J.J. Jonas, Initiation of Dynamic Recrystallization in Constant Strain Rate Hot Deformation, *ISIJ Int.*, 2003, **43**(5), p 684–691
4. S.L. Wang, M.X. Zhang, H.C. Wu, and B. Yang, Study on the Dynamic Recrystallization Model and Mechanism of Nuclear Grade 316LN Austenitic Stainless Steel, *Mater. Charact.*, 2016, **118**, p 92–101
5. C.Y. Sun, Y. Xiang, Q.J. Zhou, D.J. Politis, Z.H. Sun, and M.Q. Wang, Dynamic Recrystallization and Hot Workability of 316LN Stainless Steel, *Metals*, 2016, **6**(7), p 152–164
6. T.S. Byun, N. Hashimoto, and K. Farrell, Temperature Dependence of Strain Hardening and Plastic Instability Behaviors in Austenitic Stainless Steels, *Acta Mater.*, 2004, **52**, p 3889–3899
7. H.X. Pei, H.L. Zhang, L.X. Wang et al., Tensile Behaviour of 316LN Stainless Steel At Elevated Temperatures, *Mater. High Temp.*, 2014, **31**(3), p 198–203
8. G.E. Dieter, *Mechanical Metallurgy*, McGraw-Hill, New York, 1976
9. W.G. Dobson and D.L. Johnson, Effect of Strain Rate on Measured Mechanical Properties of Stainless Steel at 4 K, *Adv. Cryogenic Eng. Mater.*, 1984, **30**, p 185–192
10. P. Behjati, A. Kermanpur, A. Najafizadeh, and H. SamaeiBaghbadorani, Microstructural Investigation on Deformation Behavior of High Purity Fe-Cr-Ni Austenitic Alloys During Tensile Testing at Different Temperatures, *Mater. Sci. Eng., A*, 2014, **618**, p 16–21
11. W.S. Park, S.W. Yoo, M.H. Kim, and J.M. Lee, Strain-Rate Effects on the Mechanical Behavior of the AISI, 300 Series of Austenitic Stainless Steel Under Cryogenic Environments, *Mater. Des.*, 2010, **31**, p 3630–3640
12. M. Botshekan, S. Degallaix, and Y. Desplanques, Influence of Martensitic Transformation on the Low-Cycle Fatigue Behaviour of 316LN Stainless Steel at 77 K, *Mater. Sci. Eng., A*, 1997, **234–236**, p 463–466
13. J.G. Qin, C. Dai, G.J. Liao, Y. Wu, X.F. Zhu, C.J. Huang, L.F. Li, K. Wang, X.G. Shen, Z.P. Tu, and H. Ji, Tensile Test of SS 316LN Jacket With Different Conditions, *Cryogenics*, 2014, **64**, p 16–20
14. E. Nagy, V. Mertinger, F. Tranta, and J. Sólyom, Deformation Induced Martensitic Transformation in Stainless Steels, *Mater. Sci. Eng., A*, 2004, **378**, p 308–313
15. A.K. Dey, D.C. Murdoch, M.C. Mataya, J.C. Speer, and D.K. Matlock, Quantitative Measurement of Deformation-Induced Martensite in 304 Stainless Steel by x-ray Diffraction, *Scr. Mater.*, 2004, **50**, p 1445–1449
16. A. Das, S. Sivaprasad, M. Ghosh, P.C. Chakraborty, and S. Tarafder, Morphologies and Characteristics of Deformation Induced Martensite During Tensile Deformation of 304 LN Stainless Steel, *Mater. Sci. Eng., A*, 2008, **486**, p 283–286
17. H. Roy, A. Ray, K. Barat, C. Hochmuth, S. Sivaprasad, S. Tarafder, U. Glatzel, and K.K. Ray, Structural Variations Ahead of Crack Tip During Monotonic and Cyclic Fracture Tests of AISI, 304LN Stainless Steel, *Mater. Sci. Eng., A*, 2013, **561**, p 88–99

18. K. Barat, H.N. Bar, D. Mandal, H. Royc, S. Sivaprasad, and S. Tarafder, Low Temperature Tensile Deformation and Acoustic Emission Signal Characteristics of AISI304LN Stainless Steel, *Mater. Sci. Eng., A*, 2014, **597**, p 37–45

19. G.L. Huang, D.K. Matlock, and G. Krauss, Martensite Formation, Strain Rate Sensitivity, and Deformation Behavior of Type 304 Stainless Steel Sheet, *Metall. Mater. Trans. A*, 1989, **20**, p 1239–1246

20. T.S. Byun, On the Stress Dependence of Partial Dislocation Separation and Deformation Microstructure in Austenitic Stainless Steels, *Acta Mater.*, 2003, **51**(11), p 3063–3071

21. J.H. Kim, W.S. Park, M.S. Chun, J.J. Kim, J.H. Bae, M.H. Kim, and J.M. Lee, Effect of Pre-straining on Low-Temperature Mechanical Behavior of AISI, 304L, *Mater. Sci. Eng., A*, 2012, **543**, p 50–57

22. J.A. Jiménez and G. Frommeye, Analysis of the Microstructure Evolution During Tensile Testing at Room Temperature of High Manganese Austenitic Steel, *Mater. Charact.*, 2010, **61**, p 221–226

23. J. Manjanna, S. Kobayashi, Y. Kamada, S. Takahashi, and H. Kikuchi, Martensitic Transformation in SUS 316LN Austenitic Stainless Steel at Room Temperature, *J. Mater. Sci.*, 2008, **43**, p 2659–2665

24. G.V. Prasad Reddy, R. Sandhya, S. Sankaran, P. Parameswaran, and K. Laha, Creep-Fatigue Interaction Behavior of 316LN Austenitic Stainless Steel with Varying Nitrogen Content, *Mater. Des.*, 2015, **88**, p 972–982

25. S.S. Hecker, M.G. Stout, K.P. Staudhammer, and J.L. Smith, Effectsof Strain State and Strain Rate on Deformation-Induced Transformationin 304 Stainless-Steel. Part I. Magnetic Measurements and Mechanical Behavior, *Metall. Trans. A-Phys Metall Mater. Sci.*, 1982, **13**(4), p 619–626

26. V. Shrinivas, S.K. Varma, and L.E. Murr, Deformation-Induced Martensitic Characteristics in 304- Stainless and 316-Stainless Steels During Room-Temperature Rolling, *Metall. Mater. Trans. A-Phys. Metall. Mater. Sci.*, 1995, **26**(3), p 661–671

27. N. Hashimoto, S.J. Zinkle, A.F. Rowcliffe, J.P. Robertson, and S. Jitsukawa, Deformation Mechanisms in 316 Stainless Steel Irradiated at 60°C and 300°C, *J. Nucl. Mater.*, 2000, **283–287**, p 528–534

28. J.W. Brooks, M.H. Loretto, and R.E. Smallman, In Situ Observations of the Formation of Martensite in Stainless Steel, *Acta Metall.*, 1979, **27**, p 1829–1838

29. J.W. Brooks, M.H. Loretto, and R.E. Smallman, Direct Observations of Martensite Nuclei in Stainless Steel, *Acta Metall.*, 1979, **27**, p 1839–1847

30. M. Eskandari, A. Najafizadeh, and A. Kermanpur, Effect of Strain-Induced Martensite on the Formation of Nanocrystalline 316L Stainless Steel After Cold Rolling and Annealing, *Mater. Sci. Eng., A*, 2009, **519**, p 46–50

31. B.K. Choudhary, Influence of Strain Rate and Temperature on Tensile Deformation and Fracture Behavior of Type 316L(N) Austenitic Stainless Steel, *Metall. Mater. Trans. A*, 2014, **45**(1), p 302–316

32. S. Sinha, J. Szpunar, N.A.P. KiranKumar, and N.P. Gurao, Tensile Deformation of 316L Austenitic Stainless Steel Using In Situ Electron Back Scatter Diffraction and Crystal Plasticity Simulations, *Mater. Sci. Eng., A*, 2015, **637**, p 48–55

33. Z.Z. Yuan, Q.X. Dai, X.N. Cheng, K.M. Chen, L. Pan, and A.D. Wang, In Situ SEM Tensile Test of High-Nitrogen Austenitic Stainless Steels, *Mater. Charact.*, 2006, **56**, p 79–83

34. A. Sato, K. Soma, and T. Mori, Hardening Due to Pre-existing ϵ-Martensite in an Fe-30Mn-1Si Alloy Single Crystal, *Acta Metall.*, 1982, **30**, p 1901–1907

35. V. Seetharaman and R. Krishnan, Influence of the Martensitic Transformation on the Deformation Behaviour of an AISI, 316 Stainless Steel at Low Temperatures, *J. Mater. Sci.*, 1981, **16**, p 523–530

36. D. Goodchild, W.T. Roberts, and D.V. Wilson, Plastic Deformation and Phase Transformation in Textured Austenitic Stainless Steel, *Acta Metall.*, 1970, **18**, p 1137–1145

37. T.S. Byun, E.H. Lee, and J.D. Hunn, Plastic Deformation in 316LN Stainless Steel-Characterization of Deformation Microstructures, *J. Nucl. Mater.*, 2003, **321**, p 29–39

38. X.F. Li, J. Chen, L.Y. Ye, W. Ding, and P.C. Song, The Influence of Strain Rate on Tensile Characteristics of SUS304 Metastable Austenitic Stainless Steel, *Acta Metall. Sin. (Engl. Lett.)*, 2013, **26**(6), p 657–662

39. X.F. Li, J.J. Li, W. Ding, S.J. Zhao, and J. Chen, Stress Relaxation in Tensile Deformation of 304 Stainless Steel, *J. Mater. Eng. Perform.*, 2017, **26**(2), p 630–635

40. X.Y. Li, Y.J. Wei, L. Lu, K. Lu, and H.J. Gao, Dislocation Nucleation Governed Softening and Maximum Strength in Nano-Twinned Metals, *Nature*, 2010, **464**, p 877–880